infrastructures

MDPI

Article

Research on Maximum Synchronous Transfer Between Metro and Bus Considering Passenger Flow Constraint

Ziye Lan [1], Shuyi Wang [2], Yinzhu Zhao [3], Yimeng Liu [1] and Yuanwen Lai [2,*]

[1] School of Engineering, Newcastle University, Newcastle upon Tyne NE1 7RU, UK; z.lan5@newcastle.ac.uk (Z.L.); yimeng.liu@newcastle.ac.uk (Y.L.)
[2] College of Civil Engineering, Fuzhou University, Fuzhou 350116, China; syw@fzu.edu.cn
[3] Fuzhou Road Transport Development Center, Fuzhou 350008, China; 15080073813@163.com
* Correspondence: laiyuanwen@fzu.edu.cn

Abstract

Synchronous transfer has been widely studied in public transport scheduling, with most research focusing on coordination among conventional bus lines. However, with the rapid expansion of urban rail transit systems, metro–bus transfers have become increasingly important for enhancing overall urban public transport network performance. This study investigates the maximum synchronous transfer problem between metro and conventional bus services under passenger flow constraints. Considering the large transfer demand and the pulse-arrival characteristics of metro trains, a passenger waiting constraint at bus stops is incorporated to reflect capacity limitations and crowding effects. A passenger-flow-constrained maximum synchronization model is formulated to optimize bus departure times without increasing service frequency. Dongjiekou Metro Station and three surrounding pairs of bus stops are selected as a case study. Model parameters are determined through field surveys and operational data. The Grey Wolf Optimizer (GWO) and a simulated annealing–improved Grey Wolf Optimizer (SA-IGWO) are employed to solve the proposed model. The results show that both algorithms significantly improve synchronized transfer volumes by adjusting departure times without increasing service frequency. Compared with the original schedule, the SA-GWO achieves an improvement in synchronization performance ranging from 45% to 50%, outperforming the standard GWO.

Keywords: metro-bus coordination; synchronous transfer optimization; timetable synchronization; transfer capacity constraint; simulated annealing-improved grey wolf optimizer (SA-IGWO)

Academic Editor: Benedetto Barabino

Received: 15 April 2026
Revised: 11 May 2026
Accepted: 13 May 2026
Published: 15 May 2026

1. Introduction

Against the backdrop of rapid urban spatial expansion and sharply increasing travel demand, determining how to improve urban travel efficiency and promote economic development through the integration of urban public transport systems has become a crucial issue [1,2]. In recent years, buses and metro systems have become the main modes of transport for meeting residents' daily travel needs, and the increasing density of their route networks has further strengthened the connections among different stations [3–5]. With the continuous expansion of metro lines, transfers between metro and conventional buses have become increasingly frequent. Research that aims to maximize the number of synchronized arrivals has become a major hotspot in public transport transfer optimization [6]. On the one hand, adjusting transfer schedules is a low-cost optimization approach [7]. Without increasing the number of vehicles, raising service frequency, or expanding infrastructure, it is still possible to significantly improve the connection efficiency between metro and bus services simply by adjusting bus departure times. On the other hand, as the degree of synchronization between buses and the metro increases, passengers' waiting time and transfer uncertainty can be reduced. By improving the reliability of public transport services, this in turn can enhance the attractiveness of public transport [3]. Such studies seek to increase the simultaneous arrivals of different routes at transfer stations, thereby providing more transfer opportunities and improving the overall service quality of urban public transport systems.

Ceder et al. (2001) [8] proposed a transfer optimization model for conventional bus networks with the objective of maximizing the number of synchronized bus arrivals at stops. However, in this model, synchronization was required strictly at the same time point, and only the case of synchronization between two routes was considered, which is difficult to realize in actual operations. Subsequently, many scholars conducted more in-depth studies based on the research findings of Ceder et al. (2001) [8]. For example, Zhigang Liu et al. (2007) [9] studied the conventional bus network and established a maximum synchronized transfer model by introducing a synchronization coefficient and station weights to reflect the differences among routes and stops. Subsequently, Chen Xia & Huang Zhongxiang (2011) [10] incorporated the importance of different stops in the network into the model and developed a regional bus network coordination and scheduling model with the objective of maximizing the number of synchronized transfers across the entire area.

In addition, Ibarra-Rojas & Rios-Solis (2012) [11] considered the adverse effects of bus bunching in the maximum synchronized transfer problem and developed a mixed-integer optimization model. Then, in a further study, Ibarra-Rojas et al. (2016) [12] introduced time windows based on pointwise synchronization to facilitate passenger transfers and avoid vehicle bunching. They also expanded the applicability of the model to analyze transfer problems during different periods, such as peak and off-peak hours, and designed a more efficient metaheuristic algorithm for solving the model.

Similarly, Siqian Pang (2021) [13] classified synchronized transfers into two categories: those without time windows and those with time windows. The study specifically analyzed the transfer modes within hubs and proposed a method for determining the priority of multimodal synchronized transfers. These findings provide useful insights for the design of time windows and station weights.

To further quantify multiple vehicle synchronizations, Zhigang Liu et al. (2007) [9] introduced a coordination coefficient to quantify the synchronization of multiple vehicle arrivals. Building on this, BO Hai-jian et al. (2013) [14] added the maximization of the number of simultaneous arrivals as an optimization objective and developed a bi-objective optimization model. Subsequently, Nesheli et al. (2016) [15] proposed a real-time control strategy for conventional bus operations with the goal of maximizing synchronization times. This strategy aimed to reduce various types of delays during bus operations, maintain appropriate headways between consecutive trips, decrease passenger waiting times, and improve transfer efficiency. They also designed an optimization framework capable of generating operational strategies, thereby increasing the number of transfers without passenger waiting time. Tengfei Sun (2016) [16] studied the maximum synchronized transfer problem between metro lines and ensured that the passenger flow waiting for transfers in station halls remained within a reasonable range by controlling the redundancy ratio. Baoyu Hu et al. (2016) [17] further investigated the synchronized transfer problem between urban conventional buses and rural passenger transport in suburban areas. Qi Yicheng (2021) [18] considered passengers' route choice behavior during transfers and developed an optimization model that minimizes passenger travel time while maximizing the number of synchronized trips.

For studies on the impact of spatiotemporal factors on passenger synchronized transfers, Shi Yuji et al. (2023) [19] comprehensively considered actual transfer demand and the temporal variability of destination station attractiveness and constructed a dynamic transfer service gap index to analyze the spatiotemporal differences in transfer efficiency across different types of metro stations. Shen Jin et al. (2022) [20] incorporated spatiotemporal characteristics into their research on the interval prediction of metro-to-bus transfer passenger flow. To address the issue of insufficient accuracy in point prediction, they developed a PSO-DeepAR combined model, which yielded favorable prediction results. Zheng Le et al. (2023) [21] used metro-to-bus transfer volume as the dependent variable and constructed a multi-scale geographically weighted regression model, revealing the impacts and spatial heterogeneity of shared bike usage around metro stations, bus service characteristics, transfer accessibility, and metro network features on transfer demand. Recent studies have also shown that improved intelligent optimization algorithms are increasingly used in public transport research, for example in urban rail passenger flow prediction and bus travel speed prediction, with reported gains in prediction accuracy and convergence efficiency [22,23].

Existing studies on bus–metro synchronized transfers have provided important insights for improving the efficiency of multimodal trips. However, most of them mainly focus on departure timetable coordination and the increase in the number of synchronized transfers, while paying insufficient attention to the practical constraint of limited passenger-holding capacity at conventional bus stops. In practice, when a metro train arrives, a large number of transferring passengers are often released within a short period of time, imposing a pronounced pulse-like passenger flow shock on conventional bus stops [24–26]. Under such circumstances, if the objective is only to maximize the number of synchronized transfers while ignoring the capacity limits of waiting areas, the resulting optimization outcomes may overlook the temporal and spatial constraints associated with boarding and alighting, and thus may deviate from actual operating conditions.

To address this limitation, this study develops a simulated annealing–improved grey wolf optimizer (SA-IGWO) based on the GWO model, and constructs a more realistic and comprehensive maximum synchronized transfer model. Its main advantage lies in the fact that it takes into account the large and pulse-like transfer passenger flows generated after metro train arrivals, and accordingly introduces constraints on the number of transfer passengers waiting at conventional bus stops. This approach aims to improve the connection between feeder buses and metro lines so as to ensure travel efficiency while providing passengers with a more equitable and comfortable transfer flow structure, thereby alleviating pressure on congested routes. By incorporating both operational and passenger flow constraints, the SA-IGWO-based model is able not only to capture the efficiency objective of synchronized transfer coordination, but also to account for the carrying capacity of stations and the practical needs of transport management, thus making the research framework more complete and the optimization results more practically feasible [27,28].

This study seeks to extend the existing literature in three main respects: (1) by incorporating the pulse-like arrival characteristics of metro transfer passengers and the waiting-capacity constraints of conventional bus stops into synchronized transfer optimization; (2) by introducing a simulated annealing mechanism into the GWO framework to improve model solution performance; and (3) by using the Dongjiekou Station case to illustrate the application potential of the proposed framework in a realistic feeder connection setting.

2. Model Overview

2.1. Problem Description

For clarity, the main sets, parameters, and decision variables used in the model are summarized in Table 1.

Table 1. Main notation used in the model.

Symbol	Description
B	set of conventional bus transfer stops
M	set of metro trips within the study period
L	set of conventional bus routes
L_r	set of bus routes serving stop r
l, s	indices of conventional bus routes
m	index of metro trip
r	index of transfer stop
y_l^i	departure time of trip i on route l
x_{m,l_i}^r	binary variable, equal to 1 if metro trip m and bus trip l_i are synchronized at stop r; 0 otherwise
$x_{li,sj}^r$	binary variable, equal to 1 if bus trip l_i and bus trip s_j are synchronized at stop r; 0 otherwise
x_{r,l_i}^m	binary variable, equal to 1 if bus trip l_i and metro trip m are synchronized at stop r for bus-to-metro transfer; 0 otherwise
h_l	minimum headway of route l
H_l	maximum headway of route l
t_m	arrival time of metro trip m
t_{lr}	average travel time of route l to stop r
w_{mr}	walking time from metro trip m to stop r
q_m^r	transfer passenger flow generated by metro trip m at stop r
$delta_{mmax}^r$	maximum allowable waiting transfer passenger flow at stop r generated by metro trip m

For a given metro station, the public transport transfer system composed of the metro and surrounding conventional bus stops and routes can generally be defined as a topological structure G = (M, B, L). Here, $M = \{1, 2, 3, \ldots, m\}$ denotes the set of metro trips within a certain period. When the studied metro station is an intermediate or terminal station, or when same station transfers and concourse transfers are considered, the problem can be simplified to a single metro line formed by superimposing trips from two lines. In cases where inter-line transfers are realized through long connecting passages—where the distance between different metro line platforms and the station entrances varies significantly, the differences in passengers' walking times to surrounding bus stops must be considered.

$B = \{1, 2, 3, \ldots, b\}$ denotes the set of conventional bus stops within the system, and $L = \{1, 2, 3, \ldots, a\}$ denotes the set of bus routes in the system. For any stop $r \in B$, the routes passing through it can be expressed as $L_r = \{1, 2, 3, \ldots, l_r\}$. For any $l \in L$, all trips departing within the study period can be represented as the set $l_i = \{1, 2, 3, \ldots, f_l\}$. The average travel time of route l arriving at stop r is denoted as t_{lr}.

The decision variables of this study are twofold: (1) the departure time y_i^j of each trip, which determines the corresponding arrival times and serves as the focus of optimization in this paper; and (2) the synchronization indicator variable, which takes the value of 1 when synchronization occurs and 0 otherwise.

$x_{m,l_i}^r = 1$ indicates synchronization between metro trip m and bus route l, trip i, when transferring from the metro to conventional buses. Specifically, if metro trip mmm arrives at time t_m, and after a walking time of w_{mr} the passenger reaches bus stop r, bus trip l_i arrives at the stop within the time window $[0, u_{mr}]$. Otherwise, the value is 0.

$x_{l_i,s_i}^r = 1$ indicates synchronization between different bus routes when passengers transfer between them. Namely, trip i of route l arrives at transfer stop r at time t_{li}, and trip j of route s arrives within the time window $[\alpha_r, u_r]$. Otherwise, the value is 0.

$x_{r,l_i}^m = 1$ indicates synchronization between a conventional bus and the metro when passengers transfer from bus to metro. In this case, trip iii of route l arrives at stop r at time

t_{li}, and after a walking time the passenger reaches the metro concourse, where metro trip mmm arrives within the time window $[0,\ u_{rm}]$. Otherwise, the value is 0.

2.2. Constraints

2.2.1. Operational Constraints

The study period is denoted as T. In order not to affect the service level of the entire bus line and to avoid increasing the operating cost of conventional buses, the headway must not be too large or too small. If h_l and H_l represent the minimum and maximum headways of route l, respectively, then the departure times y_i^l and y_{i-1}^l of two consecutive trips on route l should satisfy

$$h_l \leq y_l^i - y_l^{i-1} \leq H_l \tag{1}$$

Specifically, when $i = 1$, that is, for the first trip of each conventional bus route within the study period, the departure must occur within the maximum headway after the start of the study period. Thus, the following conditions should be satisfied:

$$0 \leq y_l^1 \leq H_l \tag{2}$$

For the last trip of each route within the study period, the departure time $y_l^{t_l}$ should not exceed the end of the study period. Thus, the following conditions should be satisfied:

$$y_l^{f_l} \leq T \tag{3}$$

$$T - y_l^{f_l} \leq H_l \tag{4}$$

Equations from (1) to (4) ensure that the headways between two consecutive vehicles are appropriate, while also constraining the departure intervals of each route within the study period T. This prevents the operation of trips outside the study period from being affected, thereby maintaining the service level of each route without causing excessive capacity waste.

For metro trip m and bus route l, trip i, synchronization can be achieved only if the following condition is satisfied:

$$\left(y_l^i + t_{lr}\right) - t_m - w_{mr} \geq \eta\left(x_{m,l_i}^r - 1\right) \tag{5}$$

$$\left(y_l^i + t_{lr}\right) - t_m - w_{mr} \leq u_{mr} - \eta\left(x_{m,l_i}^r - 1\right) \tag{6}$$

In the equation, η is a sufficiently large number, ensuring that when a synchronization between a metro trip and a bus trip is realized, $x_{m,l_i}^r = 1$. Similarly, the synchronization between trip i of bus route l and trip j of bus route s should satisfy the following condition:

$$\left(y_l^i + t_{lr}\right) - \left(y_s^j + t_{sr}\right) \geq \alpha_r + \eta\left(x_{li,sj}^r - 1\right) \tag{7}$$

$$\left(y_l^i + t_{lr}\right) - \left(y_s^j + t_{sr}\right) \leq u_r + \eta\left(x_{li,sj}^r - 1\right) \tag{8}$$

For a bus trip i of route l and a metro trip m to be synchronized, the following condition must be satisfied:

$$t_m - \left(y_l^i + t_{lr}\right) - w_{rm} \geq \eta\left(x_{\mathrm{r},li}^m - 1\right) \tag{9}$$

$$t_m - \left(y_l^i + t_{lr}\right) - w_{rm} \leq u_{rm} - \eta\left(x_{\mathrm{r},li}^m - 1\right) \tag{10}$$

2.2.2. Passengers Constraints

When passengers transfer from the metro to conventional buses, due to differences in walking speed and the service capacity of facilities, their arrivals are concentrated within a certain time interval $[t_{min},\ t_{max}]$, which corresponds to the synchronization time window.

At present, most research [29,30] findings assume that walking time follows a normal distribution, and its probability density function is:

$$f(t) = \begin{cases} \frac{1}{\sqrt{2\pi}\sigma} \exp\left(-\frac{(t-\mu)^2}{2\sigma^2}\right) & t_{min} \leq t \leq t_{max} \\ 0 & t < t_{min} \; or \; t > t_{max} \end{cases} \tag{11}$$

By integrating the probability density function, the probability of passengers' walking time can be obtained. However, due to the limitation of the function's domain, the total probability within the defined domain is not equal to 1. Therefore, a coefficient θ needs to be added so that $p(t_{max}) = 1$, i.e., normalization is performed.

In general, passengers transferring from the metro to conventional buses tend to board the earliest arriving bus after reaching the stop. Those arriving later need to wait. Since transfer passenger flows generated by metro arrivals are pulsed in nature and metro train capacity is relatively large, if the arrival times of conventional bus trips at transfer stops are not well coordinated, this will result in significant passenger accumulation at bus stops waiting for transfers. Hence, it is necessary to adjust the departure times of different conventional bus trips.

After the arrival of metro trip mmm, the total transfer passenger flow generated at stop r is denoted as Q_m^r. Accordingly, the transfer passenger flow arriving at time t can be expressed as $q_m^r(t)$:

$$q_m^r(t) = Q_m^{\mathrm{r}} \times p(t) \tag{12}$$

The number of passengers waiting for transfer at transfer station r, denoted as $\overline{\boldsymbol{q}}_{\boldsymbol{m}}^{\boldsymbol{r}}$, is equal to the total number of arriving passengers minus the number of successful transfers.

$$\overline{q}_m^r(t) = q_m^r(t) - \sum_{\mathrm{x}=1}^{n} c_i \tag{13}$$

In the formula: n denotes the total number of bus trips arriving at the transfer stop within the time interval $[\boldsymbol{t_{min}}, \boldsymbol{t}]$ after the arrival of metro trip m. $\boldsymbol{c_i}$ represents the number of passengers successfully transferring to bus trip iii. Since conventional bus services may allow for a certain degree of overloading, this study introduces $\boldsymbol{p_l}$ as a boarding probability to represent the average probability that waiting transfer passengers can board an arriving bus. It is further assumed that all these passengers can successfully transfer, meaning that the transferable passenger flow equals the product of the total waiting passenger flow and $\boldsymbol{p_l}$. At this point, $\overline{\boldsymbol{q}}_{\boldsymbol{m}}^{\boldsymbol{r}}$ can be regarded as the residual passengers who were unable to board after the previous bus departure, plus the new transfer passengers arriving before the next bus arrival.

$$c_i = p_l \times [\overline{q}_m^r(t_{i-1}) + q_m^r(t_i) - q_m^r(t_{i-1})] \tag{14}$$

In the formula: $\boldsymbol{t_i}$ and $\boldsymbol{t_{i-1}}$ denote the arrival times at stop $\boldsymbol{r}$ of two consecutive trips.

To ensure transfer efficiency, the number of passengers waiting for transfer at the stop should be restricted within a certain range. Within a given period, passengers arriving at stop r from metro trip mmm can be divided into two groups: those who successfully transfer and those who remain waiting at the stop. The smaller the waiting passenger flow $\overline{\boldsymbol{q}}_{\boldsymbol{m}}^{\boldsymbol{r}}$, the higher the transfer efficiency. If the maximum transfer passenger flow from the metro that conventional bus stop rrr can accommodate is denoted as $\boldsymbol{\delta_{max}^r}$ then the passenger flow constraint can be expressed as:

$$\overline{q}_m^r \in [0, \delta_{\mathrm{max}}^r] \tag{15}$$

The transfer passenger flows from different metro lines, as well as from different directions of the same line, are superimposed at the conventional bus stop. At this point, the transfer passenger flow is the total flow resulting from the aggregation of transfer

https://doi.org/10.3390/infrastructures11050175

passengers generated by metro trips arriving from different lines or different directions at the conventional bus transfer stop.

2.3. Passenger-Flow-Constrained Optimization Model

Due to differences in routes and service areas, the importance of conventional bus lines in transfer connections with the metro is not uniform. To quantify this difference, proportional coefficients φ_m^l and φ_l^m are introduced, where a larger coefficient indicates a higher synchronization weight. Accordingly, the complete metro–bus maximum synchronization transfer model considering passenger flow constraints is formulated as follows:

$$\max Z = \left\{ \sum_{r\in B}\sum_{m\in M}\sum_{l\in L_r}\sum_{l_i\in l} (\varphi_m^l x_{m,l_i}^r) + \sum_{r\in B}\sum_{l\in L_r}\sum_{s\in L_r}\sum_{l_i\in l}\sum_{s_j\in s} (x_{l_i,s_j}^r) + \sum_{r\in B}\sum_{m\in M}\sum_{l\in L_r}\sum_{l_i\in l} (\varphi_l^m x_{r,l_i}^m) \right\} \tag{16}$$

$$\text{s.t. } 0 \le {y_l}^1 \le H_l, \quad \forall l \in L$$

$$y_l^{f_l} \le T, \quad \forall l \in L$$

$$T - y_l^{f_l} \le H_l, \quad \forall l \in L$$

$$h_l \le y_l^i - y_l^{i-1} \le H_l, \quad \forall l \in L, i = 1,2,\ldots,f_l$$

$$(y_l^i + t_{lr}) - t_m - w_{mr} \ge \eta(x_{m,l_i}^r - 1), \quad \forall l \in L_r, l_i \in l, m \in M, r \in B$$

$$(y_l^i + t_{lr}) - t_m - w_{mr} \le u_{mr} - \eta(x_{m,l_i}^r - 1), \quad \forall l \in L_r, l_i \in l, m \in M, r \in B$$

$$(y_l^i + t_{lr}) - (y_s^j + t_{sr}) \ge \alpha_r + \eta(x_{li,sj}^r - 1), \quad \forall l \in L_r, l_i \in l, s \in L_r, s_j \in s, m \in M, r \in B, l \ne s$$

$$(y_l^i + t_{lr}) - (y_s^j + t_{sr}) \le u_r + \eta(x_{l_i,s_j}^r - 1), \quad \forall l \in L_r, l_i \in l, s \in L_r, s_j \in s,\ m \in M, r \in B \text{ and } l \ne s$$

$$t_m - (y_l^i + t_{lr}) - w_{rm} \ge \eta(x_{\mathrm{r},li}^m - 1), \quad \forall l \in L_r, l_i \in l, m \in M, r \in B$$

$$t_m - (y_l^i + t_{lr}) - w_{rm} \le u_{rm} - \eta(x_{r,li}^m - 1), \quad \forall l \in L_r, l_i \in l, m \in M, r \in B$$

$$x_{m,li}^r \in \{0,1\}, \quad \forall l \in L_r, l_i \in l, m \in M, r \in B$$

$$x_{li,sj}^r \in \{0,1\}, \quad \forall l \in L_r, l_i \in l, s \in L_r, s_j \in s, r \in B \text{ and } l \ne s$$

$$x_{r,li}^m \in \{0,1\}, \quad \forall l \in L_r, l_i \in l, m \in M, r \in B$$

$$\overline{q}_m^r \in [0, \delta_{max}^r], \quad \forall l \in L_r, l_i \in l, m \in M, r \in B$$

3. Algorithm Improvements

3.1. The Grey Wolf Optimizer (GWO)

The Grey Wolf Optimizer (GWO) is a swarm intelligence algorithm proposed by Mirjalili et al. (2014) [31]. It is characterized by its intuitive mathematical formulation, few parameters, ease of implementation, and strong performance robustness. Inspired by the hunting behavior of grey wolves, the algorithm mainly consists of processes such as population hierarchy classification, tracking, encircling, and attacking. GWO achieves a dynamic balance between exploration and exploitation through its simple parameter structure, and demonstrates strong robustness in solving high-dimensional, complex, and nonlinear optimization problems [32]. Owing to its strong practicality and adaptability, GWO is still widely applied in optimization studies related to metro feeder connections [33,34].

3.1.1. Hierarchical Classification of the Population

In the GWO algorithm, grey wolf individuals are divided into 4 categories according to their fitness values. The three wolves with the best fitness are defined as the α wolf (the potential optimal solution), β wolf, and δ wolf, which correspond to the three best solutions to the current problem. These wolves are assumed to know the approximate location of the prey, and their positions are marked. They guide the remaining individuals (ω wolves) in updating their positions, i.e., the positions of these three wolves are used to update all individuals of the next generation. Through continuous iterations, the population gradually approaches the prey, and the hunting process—consisting of encircling, hunting, and attacking—corresponds to the optimization procedure of the algorithm.

3.1.2. Encircling the Prey

When hunting, grey wolves gradually approach and encircle their prey. The mathematical model for updating positions corresponding to this behavior is expressed as:

$$\vec{X}(\mathrm{d}+1) = \vec{X}_P(d+1) - \vec{A} \cdot \vec{D} \tag{17}$$

$$\vec{D} = \left| \vec{C} \cdot \vec{X}_P(t) - \vec{X}(t) \right| \tag{18}$$

In the formula, vector X represents the current position of a grey wolf individual, corresponding to a feasible solution of the optimization problem; d denotes the number of iterations; $\boldsymbol{X_P}$ represents the position of the prey, corresponding to the optimal solution of the problem; and D indicates the distance between the grey wolf and the prey. Vectors A and C are model parameters, and their calculation formulas are given as follows:

$$\vec{A} = 2a \cdot \vec{r_1} - a \tag{19}$$

$$\vec{C} = 2\vec{r_2} \tag{20}$$

In the formula, $\boldsymbol{r}_1$ and $\boldsymbol{r}_2$ are random vectors with dimensions identical to that of the grey wolf position, and their elements are uniformly distributed within the interval [0, 1]. Parameter $\boldsymbol{a}$ is the convergence factor used to balance the exploration and exploitation abilities of the algorithm, with a value range of [0, 2]. Its calculation formula is given as follows:

$$a = 2 - 2\left(\frac{d}{d_{max}}\right) \tag{21}$$

In the formula, $\boldsymbol{d}$ and $\boldsymbol{d_{max}}$ denote the current iteration number and the maximum number of iterations, respectively. It can be observed that the value of $\boldsymbol{a}$ decreases linearly as the number of iterations increases.

3.1.3. Hunting the Prey

In the algorithm, the actual position of the prey is unknown. Therefore, the model performs optimization based on the positions of the three leading wolves, which provides a better estimation of the prey's location. These wolves guide the movement of the other individuals and update the positions of all members in the population. This process can be mathematically expressed as:

$$\vec{X}(d+1) = \frac{\left(\vec{X}_1 + \vec{X}_2 + \vec{X}_3\right)}{3} \tag{22}$$

$$\vec{X}_1 = \vec{X}_\alpha(d) - \vec{A}_1 \cdot \vec{D}_\alpha \tag{23}$$

$$\vec{X}_2 = \vec{X}_\beta(d) - \vec{A}_2 \cdot \vec{D}_\beta \tag{24}$$

$$\vec{X}_3 = \vec{X}_\delta(d) - \vec{A}_3 \cdot \vec{D}_\delta \tag{25}$$

$$\vec{D}_{\alpha} = \left| \vec{C}_1 \cdot \vec{X}_{\alpha}(d) - \vec{X}(d) \right| \tag{26}$$

$$\vec{D}_{\beta} = \left| \vec{C}_2 \cdot \vec{X}_{\beta}(d) - \vec{X}(d) \right| \tag{27}$$

$$\vec{D}_{\delta} = \left| \vec{C}_3 \cdot \vec{X}_{\delta}(d) - \vec{X}(d) \right| \tag{28}$$

3.1.4. Attacking the Prey

At the beginning, the individuals in the population disperse to expand the search range for prey. Once suitable prey is detected, they gradually move closer to initiate an attack. As shown in Equation (19), $\boldsymbol{A}$ is a random value within the interval $[-\boldsymbol{a}, \boldsymbol{a}]$. When $|\boldsymbol{A}| \geq 1$, grey wolf individuals update their positions over a wider range, enabling the algorithm to perform a global search and thus avoid local optima to some extent. When $|\boldsymbol{A}| < 1$, grey wolf individuals continuously approach the prey, tending to launch an attack, which corresponds to local search.

3.2. Improvements to the Grey Wolf Optimizer

The GWO algorithm also has certain limitations, such as slow convergence in the later stages of iteration and a tendency to fall into local optima. In this section, improvements are introduced to the standard GWO algorithm with the aim of enhancing its performance.

3.2.1. Nonlinear Adjustment of the Convergence Factor

The parameter A is affected by the convergence factor a. In the standard algorithm, the convergence factor a decreases linearly. However, in practical problems, the search process of the algorithm is highly complex and not simply linear. A linearly decreasing convergence factor a cannot effectively balance the global and local search capabilities.

By introducing a convergence factor a that varies according to the cosine function, as shown in Equation (29), the algorithm can be improved. In the early stage of the algorithm, the value of $\boldsymbol{a}$ remains relatively large, enabling a more comprehensive search and increasing the probability of locating better solutions. In the later stage, the value of a remains small for a longer period, which allows the algorithm to converge more quickly and improves its accuracy.

$$a = \begin{cases} a_{min} + 0.5(a_{max} - a_{min})\left[1 + cos\left(\frac{(d-1)\pi}{(d_{max}-1)}\right)\right] & d \leq \frac{d_{max}}{2} \\ a_{min} + 0.5(a_{max} - a_{min})\left[1 - cos\left(\frac{(d-1)\pi}{(d_{max}-1)}\right)\right] & d > \frac{d_{max}}{2} \end{cases} \tag{29}$$

In the formula, a_{min} and a_{max} represent the lower and upper bounds of the convergence factor, which are set to 0 and 2, respectively. d and d_{max} denote the current and maximum iteration numbers of the algorithm.

3.2.2. Dynamic Adjustment of the Position Update Formula

In the Grey Wolf Optimizer, a strict hierarchical structure is imposed during the ranking process, and the optimization procedure is simulated such that higher-ranking individuals guide the lower-ranking ones through iterative search. However, in the standard algorithm, the position update formula assigns equal weights to the top three individuals. Therefore, in the improved algorithm, weight coefficients are introduced for wolves of different ranks in the position update formula to reflect their leadership roles and enable dynamic position updating. In practice, this allows better solutions to be assigned greater weights, thereby accelerating convergence. For maximization problems, the dynamic position update formula is expressed as follows:

$$w_1 = \frac{f_\alpha}{f_\alpha + f_\beta + f_\delta} \tag{30}$$

$$w_2 = \frac{f_\beta}{f_\alpha + f_\beta + f_\delta} \tag{31}$$

$$w_3 = \frac{f_\delta}{f_\alpha + f_\beta + f_\delta} \tag{32}$$

$$\vec{X}_{(t+1)} = w_1 \cdot \vec{X}_1 + w_2 \cdot \vec{X}_2 + w_3 \cdot \vec{X}_3 \tag{33}$$

In the formula, $\boldsymbol{w_1}$, $\boldsymbol{w_2}$, and $\boldsymbol{w_3}$ represent the dynamic weight coefficients of the α, β, and δ wolves, respectively, in updating the positions of the next generation. $\boldsymbol{f_\alpha}$, $\boldsymbol{f_\beta}$, and $\boldsymbol{f_\delta}$ denote the fitness values of the α, β, and δ wolves, respectively. For minimization problems, the dynamic position update formula can be modified accordingly.

3.2.3. Introduce a Simulated Annealing Operation

Simulated Annealing (SA) [35,36] is a stochastic optimization algorithm inspired by the physical process of solid annealing. In the physical annealing process, molecules in a solid possess high energy and intense thermal motion at high temperatures; as the temperature gradually decreases, the internal energy of the molecules is reduced, their motion slows down, and the system eventually reaches stability [37]. By analogy, in the algorithm, the high-temperature stage corresponds to a strong global exploration ability, enabling wide jumps across the search space. As the temperature decreases, the search range gradually narrows, favoring local fine-tuning. Meanwhile, SA introduces the Metropolis criterion to determine whether to accept a new solution: when the new solution is better than the current one, it is accepted directly; when it is worse, it is still accepted with a certain probability, thereby effectively preventing premature convergence to local optima. Based on this feature, this study incorporates the annealing mechanism into the iteration process of the improved GWO to enhance its global search capability.

$$P = \begin{cases} 1 & f(x) < f(x)' \\ \exp\left(-\frac{f(x)-f(x)'}{T_P}\right) & f(x) \geq f(x)' \end{cases} \tag{34}$$

In the formula, $\boldsymbol{f(x)}'$ denotes the fitness of the newly generated solution, $\boldsymbol{f(x)}$ represents the fitness of the current solution, and $\boldsymbol{T_p}$ is the current temperature.

3.3. Comparison of Algorithms

To verify the performance of the proposed SA-IGWO algorithm compared with the standard GWO algorithm, four benchmark test functions, denoted as $\boldsymbol{f_1}$ to $\boldsymbol{f_4}$, were selected for evaluation. The types and mathematical expressions of these functions are summarized in Table 2. For all experiments, the population size was set at 100 and the maximum number of iterations was set at 200. In addition, for the SA-IGWO algorithm, the initial temperature was set to 100, and the temperature decay coefficient was set to 0.98. The test results are illustrated in Figure 1.

Table 2. Benchmark functions.

Type	Function	Expression	Dimension	Search Range	Minimum Value
Unimodal Function	Quadric	$f_1(x) = \sum_{i=1}^{n} (\sum_{j=1}^{i} x_j)^2$	30	[−100, 100]	0

Table 2. *Cont.*

Type	Function	Expression	Dimension	Search Range	Minimum Value
Unimodal Function	Alpine	$f_2(x) = \sum_{i=1}^{n} \lvert x_i \sin x_i + 0.1x_i \rvert$	30	$[-10, 10]$	0
Multimodal Function	Rastrigin	$f_3(x) = \sum_{i=1}^{n} [x_i{}^2 - 10\cos(2\pi x_i) + 10]$	30	$[-5.12, 5.12]$	0
Multimodal Function	Ackley	$f_4(x) = -20\exp(-0.2\sqrt{\frac{1}{n}\sum_{i=1}^{n} x_i{}^2}) - \exp[\frac{1}{n}\sum_{i=1}^{n}\cos(2\pi x_i)] + 20 + e$	30	$[-32, 32]$	0

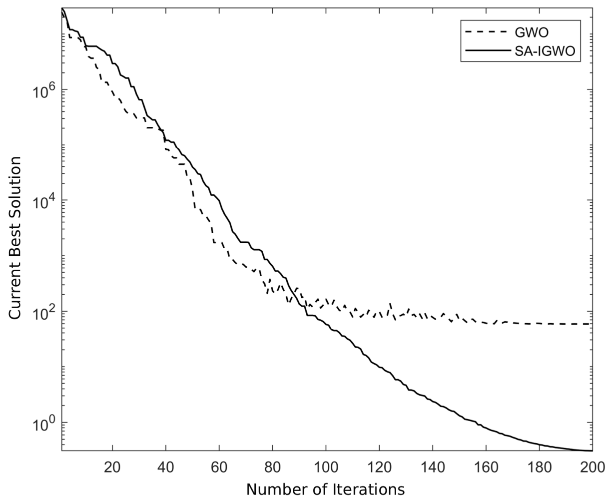

(**a**). Test function $f_1(x)$

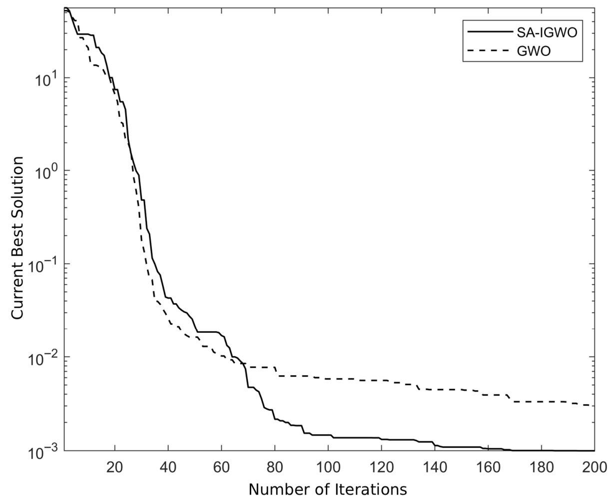

(**b**). Test function $f_2(x)$

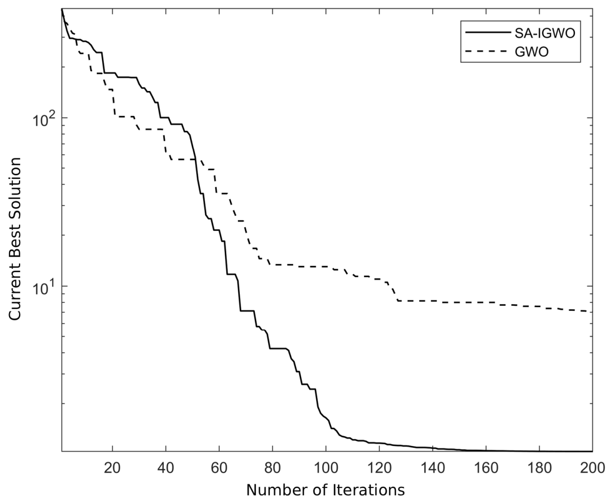

(**c**). Test function $f_3(x)$

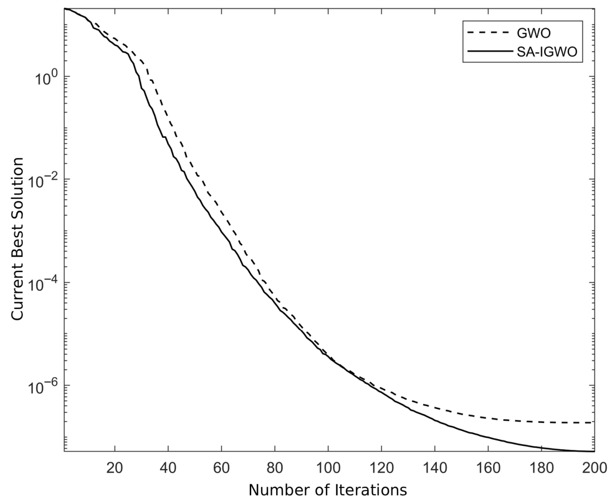

(**d**). Test function $f_4(x)$

Figure 1. Comparison of iterative results of test functions.

As shown in Figure 1, the SA-IGWO exhibits comparable exploration capability in the early iterations and demonstrates significantly faster convergence and higher solution accuracy in the middle and later stages compared with the standard GWO. Due to the introduction of the simulated annealing mechanism, the runtime of SA-IGWO increases by approximately 3–5% relative to the standard GWO. However, this marginal increase does not substantially affect computational complexity, while it significantly enhances convergence speed and solution quality. Simulation results further indicate that SA-IGWO consistently outperforms GWO, thereby validating the effectiveness and robustness of the proposed SA-IGWO algorithm.

4. Case Study

This study selects the weekday evening peak period from 17:00 to 18:00 as the research interval, during which the departure timetables of bus services within the study area is optimized. The parameter setting in this case study is based on a combination of field survey observations and operational data. Specifically, the data from 17:00 to 18:00 are mainly used to derive operational parameters such as bus running times, headways, and the number of trips; the field survey conducted from 17:00 to 19:00 mainly records metro arrival times and the times at which transferring passengers reach the bus stops, so as to identify the interval characteristics of passengers' transfer walking times under evening-peak conditions and provide the basis for estimating transfer time windows; the passenger-flow survey conducted from 18:00 to 19:00 mainly records the number of metro alighting passengers and the number transferring to conventional buses, and is used to calibrate the stop-level upper limit of passenger-flow constraints by estimating the proportion and directional differences of metro alighting passengers transferring to conventional buses. Both the 17:00–19:00 and 18:00–19:00 surveys fall within adjacent weekday evening-peak periods, and their results are therefore considered to reflect the same peak-period operating context.

4.1. Research Objects

Dongjiekou Station was selected as the case study site because it is a relatively high-demand station in the Fuzhou metro network and is surrounded by multiple conventional bus stops and routes, forming a representative and operationally complex metro–bus transfer environment. In addition, its central urban location makes it suitable for both field investigation and parameter calibration.

As of August 2023, a total of five metro lines with 92 stations have been opened and put into operation in Fuzhou. Dongjiekou Station, located on Metro Line 1, is one of the stations with relatively high passenger volumes in the Fuzhou metro network. By using relevant software, the arrival times of both metro services and conventional bus routes at Dongjiekou Station during the study period can be accurately obtained.

According to the official website of Fuzhou Metro, Dongjiekou Station has four entrances and exits (labeled A through D). The surrounding conventional bus stops include Dongjiekou, Gulou, and Nan Street, comprising three pairs of bus stops and a total of 25 bus routes. Since the GPS records of conventional buses do not necessarily correspond to the actual operating directions of different routes, the bus routes are classified according to the stops they pass through. The bus routes are divided into inbound and outbound directions, where the stops along the route are generally the same (with slight differences for a few routes), but the terminal stations are opposite. Because a single bus route may pass through multiple transfer stops around the metro, the first stop it passes is selected as the transfer stop for that route in this study. The inbound and outbound directions are kept consistent with the GPS data used in this study. The selected transfer stops for each route are shown in Table 3.

Table 3. Line table of conventional bus station.

Stop	Bus Routes
Dongjiekou 1 stop	Routes 5, 19, 22, 27 *, 55 *, 118 *, 301 *, 317 *, and 327 *.
Dongjiekou 2 stop	Routes 5 *, 22 *, 27, 55, 74, 80, 88, 102, 117 *, 118, 301, 310, 317, 327
Gulou 1 stop	Routes 8 *, 18 *, 19 *, 20 *, 61 *, 74 *, 75, 80 *, 88 *, 101 *, 102 *, 121 *, 128, 310
Gulou 2 stop	Routes 18, 61 *, 75 *, 128 *
Nanjie 1 stop	Routes 1, 8, 20, 66,101, 117, 121
Nanjie 2 stop	Routes 1 *, 66 *

Note: An asterisk (*) indicates the outbound direction.

4.1.1. Transfer Time

In this study, field investigations were conducted to record the arrival times of metro trips and the arrival times of transfer passengers at conventional bus stops during the evening weekday peak period (17:00–19:00), in order to determine the connection time window for passengers transferring from the metro to conventional buses. Specifically, transfer passenger flow data for 10 bus trips were recorded at each conventional bus stop, and the walking time interval was obtained by taking the upper and lower bounds of the data, averaging, and rounding.

The process of transferring from conventional buses to the metro is similar. However, since a single conventional bus trip generates relatively fewer transfer passengers, their arrival times at the metro platform are more concentrated. Subsequently, the recorded walking time data of transfer passengers from the metro to each conventional bus stop were fitted with a normal distribution function. The mean value μ of the normal distribution was taken as the average, and a 2 min time range was defined as the length of the time window. That is, using the mean as the center, a $\pm$ 1 min interval was applied to obtain the time window for passengers transferring from conventional buses to the metro, as shown in Table 4.

Table 4. Time window of transfer passenger flow.

Stop	Transfer Time Window from Metro to Bus (min)				Transfer Time Window from Bus to Metro (min)			
	A Exit	B Exit	C Exit	D Exit	A Exit	B Exit	C Exit	D Exit
Dongjiekou 1 Stop	-	-	-	[4.0, 7.0]	-	-	-	[4.6, 6.6]
Dongjiekou 2 Stop	[5.0, 8.0]	-	-	-	[5.8, 7.8]	-	-	-
Gulou 1 Stop	-	[6.0, 9.0]	-	-	-	[6.0, 8.0]	-	-
Gulou 2 Stop	[5.0, 9.0]	-	-	-	[5.7, 7.7]	-	-	-
Nanjie 1 Stop	-	-	-	[4.0, 7.0]	-	-	-	[4.6, 6.6]

Passenger arrival time during transfers between different conventional bus routes is approximately equal to the bus arrival time. For transfers from conventional buses to the metro, passengers need additional time to alight. If buses from different routes arrive within an extremely short interval, bus bunching may occur, which wastes capacity, reduces operational safety, and increases safety risks for passengers. To avoid this, 0.5 min are added to the conventional synchronized time window, resulting in a synchronized transfer time window of [0.5, 2.5] between conventional buses.

4.1.2. Conventional Bus Headways, Trips, and Arrival Times

Based on the GPS operation data of Fuzhou Bus Company collected over one week of weekdays, we recorded and obtained the operating time required for each bus route to reach the transfer stops within the study area during 17:00–18:00, as well as the upper and lower bounds of departure frequency and departure intervals, as shown in Table 5.

Table 5. Related parameters of conventional bus lines.

Upbound Route	Arrival Stop	Travel Time (min)	Headway (min)	Number of Trips	Downbound Route	Arrival Stop	Travel Time (min)	Headway (min)	Arrival Stop
Route 1	Nanjie 1 Stop	39.6	[5, 15]	7	Route 1 *	Nanjie 2 Stop	16.7	[5, 15]	7
Route 5	Dongjiekou 1 Stop	44.7	[5, 12]	5	Route 5 *	Dongjiekou 2 Stop	22.5	[5, 12]	6
Route 8	Nanjie 1 Stop	34.5	[3, 10]	9	Route 8 *	Gulou 1 Stop	36.5	[3, 10]	9
Route 18	Gulou 2 Stop	57.1	[5, 14]	7	Route 18 *	Gulou 1 Stop	20.9	[5, 14]	7
Route 19	Dongjiekou 2 Stop	39.8	[5, 12]	9	Route 19 *	Gulou 1 Stop	45.0	[5, 12]	9
Route 20	Nanjie 1 Stop	29.1	[6, 10]	7	Route 20 *	Gulou 1 Stop	42.2	[6, 10]	8
Route 22	Dongjiekou 1 Stop	23.0	[6, 10]	7	Route 22 *	Dongjiekou 2 Stop	27.7	[6, 10]	7
Route 27	Dongjiekou 2 Stop	42.8	[5, 12]	7	Route 27 *	Dongjiekou 1 Stop	28.4	[10, 20]	4
Route 55	Dongjiekou 2 Stop	35.3	[5, 10]	7	Route 55 *	Dongjiekou 1 Stop	49.0	[5, 10]	6
Route 61	Gulou 1 Stop	31.1	[10, 20]	4	Route 61 *	Gulou 2 Stop	42.7	[10, 20]	5
Route 66	Nanjie 1 Stop	40.6	[10, 20]	4	Route 66 *	Nanjie 2 Stop	35.2	[10, 15]	6
Route 74	Dongjiekou 2 Stop	51.0	[7, 15]	6	Route 74 *	Gulou 1 Stop	31.1	[10, 20]	4
Route 75	Gulou 1 Stop	38.7	[7, 15]	6	Route 75 *	Gulou 2 Stop	29.3	[7, 15]	6
Route 80	Dongjiekou 2 Stop	54.9	[5, 12]	6	Route 80 *	Gulou 1 Stop	31.5	[5, 12]	6
Route 88	Dongjiekou 2 Stop	44.3	[10, 20]	4	Route 88 *	Gulou 1 Stop	25.7	[10, 20]	5
Route 101	Nanjie 1 Stop	40.7	[5, 12]	8	Route 101 *	Gulou 1 Stop	32.8	[5, 12]	6
Route 102	Dongjiekou 2 Stop	46.7	[7, 12]	6	Route 102 *	Gulou 1 Stop	36.4	[7, 12]	9
Route 117	Nanjie 1 Stop	48.7	[3, 12]	6	Route 117 *	Dongjiekou 2 Stop	41.0	[3, 12]	6
Route 118	Dongjiekou 2 Stop	46.6	[5, 15]	6	Route 118 *	Dongjiekou 1 Stop	27.8	[5, 15]	9

Note: An asterisk (*) indicates the outbound direction.

Table 5. *Cont.*

Upbound Route	Arrival Stop	Travel Time (min)	Headway (min)	Number of Trips	Downbound Route	Arrival Stop	Travel Time (min)	Headway (min)	Arrival Stop
Route 121	Nanjie 1 Stop	57.4	[5, 10]	8	Route 121 *	Gulou 1 Stop	34.6	[5, 10]	7
Route 128	Gulou 1 Stop	31.1	[5, 12]	6	Route 128 *	Gulou 2 Stop	52.9	[5, 12]	7
Route 301	Dongjiekou 2 Stop	51.3	[7, 12]	6	Route 301 *	Dongjiekou 1 Stop	13.9	[7, 12]	7
Route 310	Dongjiekou 2 Stop	21.4	[7, 15]	7	Route 310 *	Gulou 1 Stop	53.0	[7, 15]	6
Route 317	Dongjiekou 2 Stop	33.6	[6, 15]	7	Route 317 *	Dongjiekou 1 Stop	54.6	[6, 15]	7
Route 327	Dongjiekou 2 Stop	26.1	[4, 10]	8	Route 327 *	Dongjiekou 1 Stop	52.5	[4, 10]	8

Note: An asterisk (*) indicates the outbound direction.

4.1.3. Passenger Flow Constraint Upper Limit

To determine the number of passengers transferring from the Dongjiekou metro station to conventional buses and the proportion of this transfer flow relative to the total number of alighting passengers, we conducted a survey during weekdays from 18:00 to 19:00. Specifically, we recorded the metro trips and the total number of alighting passengers, while simultaneously collecting data on the number of transfer passengers at the conventional bus stops. The statistical results are shown in Table 6. The survey data indicate that the total number of alighting passengers during the survey period was 2803, of which 549 transferred to conventional buses, accounting for 19.58%. Furthermore, the total alighting passenger flow and the number of transfers to conventional buses from Sanjiangkou to Xiangfeng were approximately twice those from Xiangfeng to Sanjiangkou. In this study, the total alighting passenger flow during the weekday peak hour at Dongjiekou Station is assumed to be 3000 passengers per hour, with 2000 passengers per hour from Sanjiangkou to Xiangfeng and 1000 passengers per hour in the opposite direction. The proportion of passengers transferring to conventional buses is set at 20% for both directions. Accordingly, the number of passengers transferring to conventional buses per metro trip in the two directions is calculated to be 36 and 16, respectively.

Table 6. Passenger flow statistics of Dongjiekou Station during weekday peak hours.

Metro Trip	The Direction from Xiangfeng to Sanjiangkou		The Direction from Sanjiangkou to Xiangfeng	
	Number of Alighting Passengers	Number of Passengers Transferring to Conventional Buses	Number of Alighting Passengers	Number of Passengers Transferring to Conventional Buses
1	97	19	152	27
2	69	13	167	32
3	62	13	175	35
4	75	15	150	33
5	77	13	149	29
6	58	11	169	34
7	87	19	193	37
8	79	16	175	33

Table 6. *Cont.*

Metro Trip	The Direction from Xiangfeng to Sanjiangkou		The Direction from Sanjiangkou to Xiangfeng	
	Number of Alighting Passengers	Number of Passengers Transferring to Conventional Buses	Number of Alighting Passengers	Number of Passengers Transferring to Conventional Buses
9	106	24	159	29
10	88	17	186	37
11	75	15	174	35
12	81	13	-	-
Sum	954	188	1849	361

At the same time, we categorized the transfer passenger flow to conventional buses by station and obtained the proportion for each transfer stop. Subsequently, we investigated the waiting areas of the transfer stops, assuming a static demand area of 1.2 m^2 per passenger. Considering that, in addition to passengers transferring from the metro, there are also passengers transferring between conventional bus routes as well as non-transfer passengers generated from surrounding areas near some stops, the calculated results were appropriately reduced. In this way, the maximum number of waiting passengers (that the upper limit of transfer waiting passenger flow) available for metro-to-bus transfers was determined, as shown in the Table 7.

Table 7. Upper Limit of Passenger Flow Constraints at Conventional Bus Stations.

Stop	Dongjiekou 1 Stop	Dongjiekou 2 Stop	Gulou 1 Stop	Gulou 2 Stop	Nanjie 1 Stop	Nanjie 2 Stop
Transfer proportion (%)	30	13	28	11	13	5
Effective waiting area (m^2)	15	8	12	20	16	22
Max. transfer waiting passengers	8	4	6	10	8	11

4.1.4. Proportional Coefficient

The smaller the overlap coefficient between the metro and conventional bus routes, the higher the value of synchronized transfers. The Dongjiekou Station studied in this paper is located at a crossroads. When passengers transfer from the metro to conventional buses, the directions of bus routes after passing the surrounding transfer stops of Dongjiekou Station can be classified into two categories: (1) routes whose directions are consistent with the metro line and (2) routes whose directions are perpendicular to the metro line. Based on this distinction, the proportional coefficients for synchronized transfers between the two categories of bus routes and the metro station are set to 1 and 2, respectively. When passengers transfer from conventional buses to the metro, the transfer flow originates from stops before the transfer station. In this case, the proportional coefficient depends on the direction of the bus route segment before reaching the transfer stop. If the direction of the bus route segment before the transfer stop is consistent with that of the metro line, the coefficient is set to 1; if it is perpendicular, the coefficient is set to 2. The detailed data are shown in Table 8.

Table 8. Transfer Ratio Coefficient.

Upbound Route	Proportional Coefficient φ_m^l	Proportional Coefficient φ_l^m	Downbound Route	Proportional Coefficient φ_m^l	Proportional Coefficient φ_l^m
Route 1	1	1	Route 1 *	1	1
Route 5	2	2	Route 5 *	2	2
Route 8	1	1	Route 8 *	1	1
Route 18	1	2	Route 18 *	2	1
Route 19	1	2	Route 19 *	2	1
Route 20	1	1	Route 20 *	1	1
Route 22	2	2	Route 22 *	2	2
Route 27	2	2	Route 27 *	2	2
Route 55	2	2	Route 55 *	2	2
Route 61	2	1	Route 61 *	1	2
Route 66	1	1	Route 66 *	1	1
Route 74	1	2	Route 74 *	2	1
Route 75	2	1	Route 75 *	1	2
Route 80	1	2	Route 80 *	2	1
Route 88	1	2	Route 88 *	2	1
Route 101	1	1	Route 101 *	1	1
Route 102	1	2	Route 102 *	2	1
Route 117	2	1	Route 117 *	1	2
Route 118	2	2	Route 118 *	2	2
Route 121	1	1	Route 121 *	1	1
Route 128	1	1	Route 128 *	1	1
Route 301	2	2	Route 301 *	2	2
Route 310	1	2	Route 310 *	2	1
Route 317	2	2	Route 317 *	2	2
Route 327	2	2	Route 327 *	2	2

Note: An asterisk (*) indicates the outbound direction.

4.2. Modeling and Analysis

The objective of this study is to generate the departure timetables of conventional bus routes within the study area, so as to achieve maximum synchronization of the transfer system composed of metro and conventional buses, under the constraints of service frequency and passenger flow. The dimensionality of the grey wolf position corresponds to the total number of departures of all bus routes within the study period and study area, denoted as vector $\vec{y} = \left\{y_1^1, y_1^2, \ldots, y_1^{f_1}, y_2^1, y_2^2, \ldots, y_2^{f_2}, \ldots, y_l^1, y_l^2, \ldots, y_l^{f_l}\right\}$, where each departure interval of a route constitutes one dimension of the grey wolf position. Based on the synchronization model established in this study, when bus routes within the study area are scheduled to depart at equal intervals during the study period, the total synchronization count at Dongjiekou Station is 1385.

To compare the performance of the proposed SA-IGWO algorithm with that of the standard GWO algorithm in solving the model developed in this study, both algorithms were applied, and their results and processes were analyzed to evaluate their relative strengths and weaknesses. The population size for both algorithms was set to 200, and the maximum number of iterations was set to 500. In addition, for the annealing operation of the SA-IGWO algorithm, the initial temperature was set to 100 and the temperature decay coefficient to 0.98. Since the proposed model involves high dimensionality and the results of each iteration are subject to randomness, each algorithm was run 10 times to provide a more comprehensive comparison. The results were also compared with the synchronization count obtained under equal-interval scheduling, as shown in Table 9. In the table, the optimization rate refers to the improvement relative to equal-interval scheduling, and the variation refers to the deviation of each run from the average result. Figure 3 illustrates part of the iteration process, where (a) and (b) show the best and worst iteration results of the SA-IGWO algorithm, respectively, and (c) and (d) show the best and worst iteration results of the GWO algorithm, respectively.

Compared with the equal-interval scheduling scheme, the optimization results of both algorithms show a significant increase in the number of synchronizations. To provide a clearer comparison of the performance differences, the results of multiple runs are presented in the form of boxplots, as shown in Figure 2.

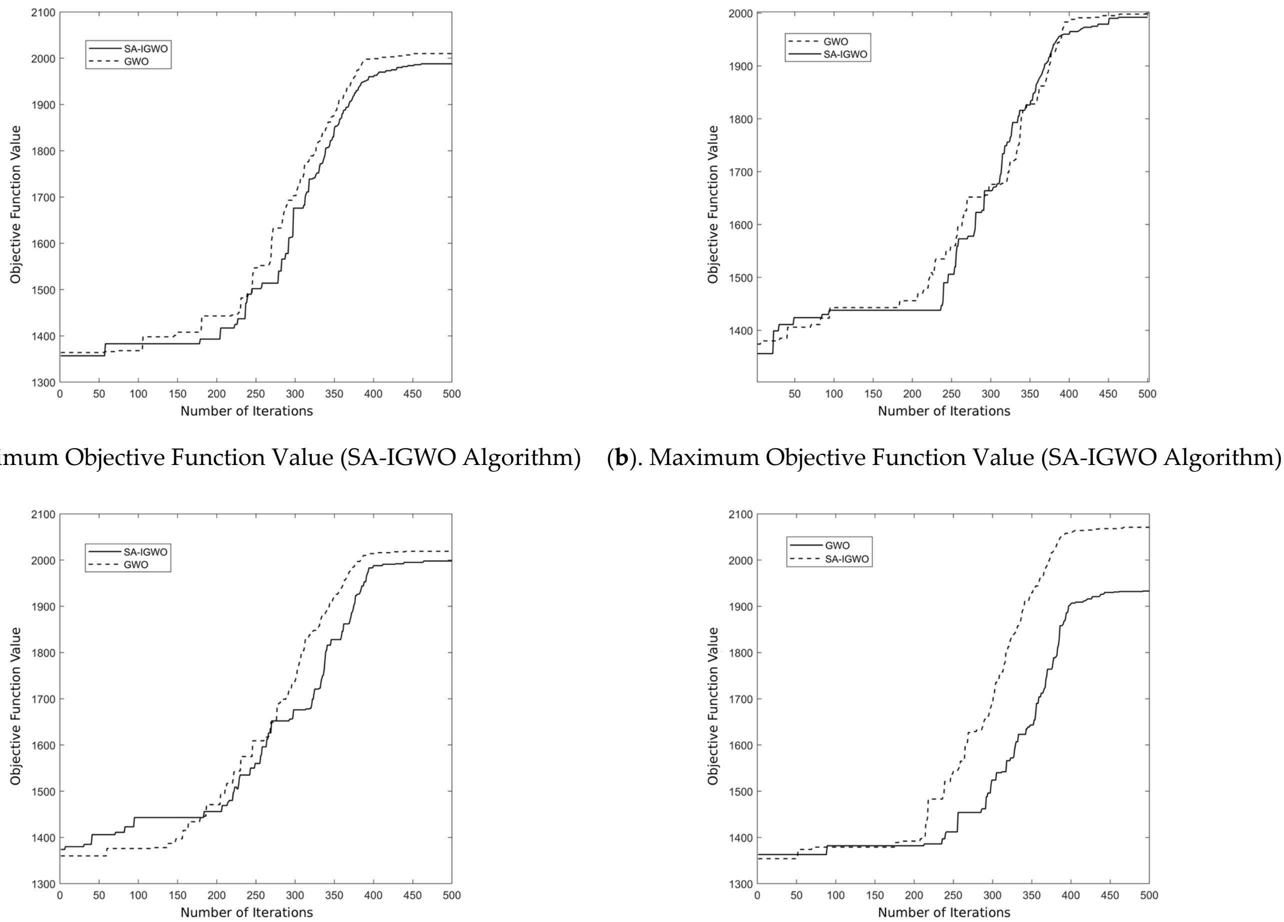

(**a**). Minimum Objective Function Value (SA-IGWO Algorithm) (**b**). Maximum Objective Function Value (SA-IGWO Algorithm)

(**c**). Minimum Objective Function Value (GWO Algorithm) (**d**). Maximum Objective Function Value (GWO Algorithm)

Figure 2. SA-IGWO and GWO iterative graphs.

For the SA-IGWO algorithm, the optimization results yield an average of 2029, with a maximum of 2073 (optimization rate of 50%) and a minimum of 2006 (optimization rate of 45%). For the GWO algorithm, the optimization results yield an average of 1985, with a maximum of 2048 (optimization rate of 48%) and a minimum of 1933 (optimization rate of 40%).

The comparative analysis of the GWO and SA-IGWO algorithms yields several important insights. First, both algorithms demonstrate strong global search capabilities and are able to achieve rapid convergence toward optimal solutions. Second, owing to the high dimensionality of the optimization problem, some variability is observed across iterations under fixed population size and iteration limits. Third, although the objective function exhibits slower improvement in the early stages for both algorithms, the incorporation of the simulated annealing mechanism in SA-IGWO significantly enhances its ability to escape local optima. Moreover, the improved position update formula and adaptive convergence factor further accelerate convergence in later stages, resulting in superior overall optimization performance compared to the standard GWO algorithm.

Table 9. Comparison of run results.

Number of Runs	Number of Synchronizations		Optimization Rate		Fluctuation Rate	
	SA-IGWO	GWO	SA-IGWO	GWO	SA-IGWO	SA-IGWO
1	2073	1961	50%	42%	2.2%	−1.2%
2	2039	1985	47%	43%	0.5%	0
3	2061	1933	49%	40%	1.6%	−2.6%
4	2008	1988	45%	44%	−1.0%	0.2%
5	2006	2048	45%	48%	−1.1%	3.2%
6	2013	2006	45%	45%	−0.8%	1.1%
7	2031	1993	47%	44%	−1.0%	0.4%
8	2016	1965	46%	42%	−0.6%	−1.0%
9	2019	1976	46%	43%	−0.5%	−0.5%
10	2026	1994	46%	44%	−0.1%	0.5%
Mean	2029	1985	46%	43%	-	-

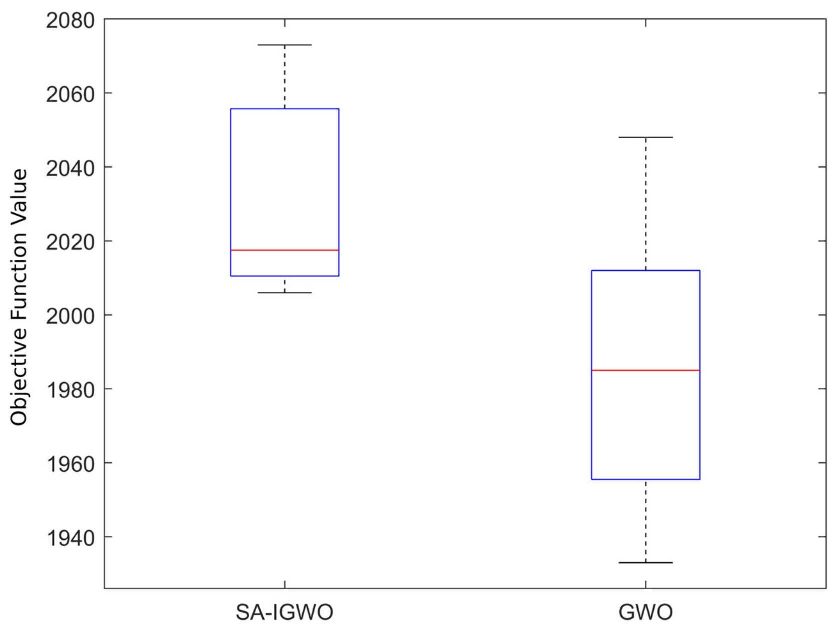

Figure 3. Iterative result box comparison graph. (The blue boxes indicate the interquartile ranges, the red lines indicate the median values, and the black dotted lines indicate the whiskers of the distribution).

Considering that actual bus timetables are generally expressed in integers, the optimal results obtained from the optimization were rounded to the nearest integer to generate the departure timetable for the conventional bus feeder routes around Dongjiekou Metro Station, as shown in Table 10. Since actual bus timetables are typically published in integer-minute form, the continuous optimization results were rounded to the nearest integer to generate the final timetable shown in Table 10. The rounded timetable is mainly intended to reflect the practical format of timetable presentation.

Table 10. Regular bus route 17:00–18:00 departure schedule.

Route	Departure Time								
Route 1	17:03	17:08	17:18	17:32	17:43	17:50	17:59		
Route 1 *	17:06	17:14	17:22	17:33	17:42	17:50	17:55		
Route 5	17:10	17:21	17:31	17:42	17:53				
Route 5 *	17:08	17:17	17:28	17:36	17:43	17:53			
Route 8	17:04	17:07	17:15	17:22	17:31	17:37	17:42	17:49	17:56
Route 8 *	17:03	17:07	17:19	17:21	17:25	17:31	17:42	17:48	17:58
Route 18	17:03	17:10	17:16	17:21	17:28	17:39	17:51		
Route 18 *	17:07	17:12	17:20	17:31	17:36	17:47	17:59		
Route 19	17:07	17:11	17:17	17:27	17:36	17:42	17:48	17:53	17:58
Route 19 *	17:04	17:10	17:14	17:19	17:28	17:33	17:35	17:41	17:56
Route 20	17:03	17:11	17:17	17:26	17:35	17:43	17:53		
Route 20 *	17:06	17:12	17:18	17:28	17:31	17:39	17:48	17:57	
Route 22	17:04	17:12	17:20	17:30	17:37	17:46	17:54		
Route 22 *	17:17	17:25	17:34	17:38	17:40	17:48	17:51		
Route 27	17:05	17:14	17:25	17:34	17:41	17:44	17:54		
Route 27 *	17:09	17:23	17:41	17:46					
Route 55	17:05	17:13	17:22	17:31	17:38	17:42	17:52		
Route 55 *	17:08	17:18	17:25	17:29	17:37	17:53			
Route 61	17:09	17:20	17:37	17:56					
Route 61 *	17:06	17:19	17:34	17:45	17:57				
Route 66	17:05	17:20	17:32	17:50					
Route 66 *	17:04	17:15	17:27	17:38	17:49	17:59			
Route 74	17:05	17:17	17:22	17:27	17:33	17:49			
Route 74 *	17:05	17:20	17:30	17:48					
Route 75	17:08	17:16	17:24	17:41	17:46	17:50			
Route 75 *	17:10	17:19	17:27	17:39	17:47	17:56			
Route 80	17:08	17:17	17:27	17:43	17:50	17:54			
Route 80 *	17:11	17:18	17:25	17:38	17:46	17:56			
Route 88	17:07	17:22	17:42	17:50					
Route 88 *	17:13	17:25	17:36	17:47	17:53				
Route 101	17:10	17:19	17:23	17:31	17:41	17:43	17:51	17:57	
Route 101 *	17:10	17:22	17:26	17:34	17:40	17:52			
Route 102	17:09	17:21	17:28	17:39	17:45	17:55			
Route 102 *	17:07	17:16	17:25	17:27	17:36	17:42	17:47	17:52	17:59
Route 117	17:08	17:21	17:27	17:30	17:37	17:58			
Route 117 *	17:09	17:15	17:24	17:35	17:44	17:54			
Route 118	17:05	17:21	17:28	17:40	17:43	17:52			
Route 118 *	17:05	17:12	17:18	17:26	17:35	17:41	17:46	17:54	18:00
Route 121	17:01	17:06	17:16	17:22	17:29	17:38	17:53	17:57	
Route 121 *	17:06	17:13	17:22	17:31	17:37	17:47	17:54		
Route 128	17:11	17:22	17:31	17:40	17:48	17:54			
Route 128 *	17:02	17:08	17:19	17:27	17:35	17:43	17:50		

Table 10. *Cont.*

Route	Departure Time							
Route 301	17:04	17:15	17:26	17:35	17:44	17:54		
Route 301 *	17:10	17:17	17:27	17:30	17:41	17:45	17:55	
Route 310	17:02	17:13	17:25	17:35	17:43	17:52	17:59	
Route 310 *	17:05	17:14	17:20	17:26	17:33	17: 51		
Route 317	17:10	17:23	17:33	17:41	17:43	17:51	17:58	
Route 317 *	17:07	17:15	17:26	17:28	17:38	17:45	17:56	
Route 327	17:02	17:08	17:17	17:24	17:31	17:40	17:47	17:56
Route 327 *	17:06	17:14	17:22	17:29	17:35	17:43	17:50	17:58

Note: An asterisk (*) indicates the outbound direction.

5. Conclusions

In investigating the problem of maximum synchronized transfers, this study takes into account the fact that transfer passenger flows generated by metro train arrivals are both large in volume and pulse-like in nature. Accordingly, constraints on the number of transfer passengers waiting at conventional bus stops are introduced, and a maximum synchronized transfer model is established that comprehensively considers both metro–bus mutual transfers and internal transfers among conventional bus services. To address the shortcomings of the GWO algorithm, this study further improves it by incorporating a simulated annealing mechanism and proposes the SA-IGWO algorithm, which is then applied in a case study.

Taking the transfer system composed of Dongjiekou Metro Station in Fuzhou and three pairs of surrounding conventional bus stops as an example, this study conducts an empirical analysis for the weekday evening peak period from 17:00 to 18:00. The results show that the proposed model and algorithm have strong practical value. Specifically, (1) under the operational and passenger flow constraints, when conventional buses adopt an equal-headway departure timetable, the total number of synchronized transfers in the system is 1385; after optimization, both algorithms can significantly improve the synchronization level of the transfer system without increasing the number of bus departures. (2) In terms of model performance, the SA-IGWO algorithm overall outperforms the GWO algorithm. The former achieves an average of 2029 synchronized transfers, with a maximum of 2073 and a minimum of 2006, corresponding to an optimization rate of 45–50%; the latter achieves an average of 1985, with a maximum of 2048 and a minimum of 1933, corresponding to an optimization rate of 40–48%. (3) Furthermore, the average number of synchronized transfers obtained by SA-IGWO is 644 higher than that under the equal-headway scheme and 44 higher than the average result of GWO. This indicates that, by introducing a simulated annealing mechanism and improving the convergence factor and position updating formulas, the algorithm's ability to escape local optima and perform refined search in the later stages is enhanced, thereby enabling it to obtain a better bus departure timetable. The improvement in synchronization can be explained as an increase in the number of transfer opportunities achieved within the predefined synchronization time windows. In practical terms, this indicates that, by adjusting bus departure times, the temporal coordination between metro arrivals and feeder bus departures has been improved, which may help reduce the likelihood of missed connections and alleviate short-term passenger accumulation at transfer stops during peak periods.

Moreover, the introduction of the passenger flow constraint changes the optimization focus of the model. The resulting timetable no longer aims only at maximizing synchronization opportunities, but also considers the stop-level carrying-capacity boundary under peak-period conditions. As a result, the optimized timetable is more consistent with practical operating conditions [38].

Overall, this study demonstrates that, without increasing vehicle supply or service frequency, the efficiency of metro–bus feeder connections can be effectively improved simply by optimizing bus departure times. At the same time, by incorporating the upper limit of waiting passenger flow as a constraint, the optimization results not only focus on maximizing the number of synchronized transfers, but also consider station carrying capacity and practical operational feasibility, making the model more consistent with real-world operating conditions.

This study still has several limitations that should be acknowledged. First, the present analysis is mainly based on deterministic parameters, whereas in actual operations, metro delays, road congestion, and fluctuations in passenger arrival times may all affect synchronized transfer performance. Therefore, the proposed framework is not yet able to fully capture the uncertainty of real operating environments. Second, the model is validated only through a single case study, namely Dongjiekou Metro Station and its surrounding feeder bus stops, which to some extent limits the generalizability of the findings to other stations or cities with different passenger demand levels, stop layouts, feeder structures, and operating conditions. Future research could further introduce robust optimization or multi-objective optimization approaches, extend the analysis to multiple stations, multiple time periods, or even regional bus–rail networks, and incorporate additional robustness tests so as to improve the broader applicability and transferability of the model [32].

Author Contributions: Conceptualization, Z.L., S.W., Y.Z. and Y.L. (Yuanwen Lai); methodology, Z.L., S.W., Y.Z. and Y.L. (Yuanwen Lai); software, Z.L., Y.Z. and Y.L. (Yuanwen Lai); validation, Z.L. and Y.Z.; formal analysis, Z.L., S.W. and Y.Z.; investigation, S.W., Y.Z. and Y.L. (Yuanwen Lai); resources, Z.L. and Y.L. (Yuanwen Lai); data curation, Z.L. and Y.L. (Yuanwen Lai); writing—original draft preparation, Z.L., S.W., Y.Z. and Y.L. (Yimeng Liu); writing—review and editing, Z.L., S.W., Y.L. (Yimeng Liu) and Y.L. (Yuanwen Lai); visualization, Z.L., Y.Z. and Y.L. (Yuanwen Lai); supervision, S.W. and Y.L. (Yuanwen Lai); project administration, Z.L., S.W. and Y.L. (Yuanwen Lai); funding acquisition, S.W. and Y.L. (Yuanwen Lai) All authors have read and agreed to the published version of the manuscript.

Funding: This research received no external funding.

Data Availability Statement: The data presented in this study are available from the corresponding author upon reasonable request.

Conflicts of Interest: The authors declare no conflict of interest.

References

1. Guo, X.; Du, Q.; Li, Y.; Zhou, Y.; Wang, Y.; Huang, Y.; Martinez-Pastor, B. Cascading Failure and Recovery of Metro–Bus Double-Layer Network Considering Recovery Propagation. *Transp. Res. D Transp. Environ.* **2023**, *122*, 103861. [CrossRef]
2. Sun, S.; Guo, X.; Sun, H. Optimization of Bus Bridging Strategy for Two Bus Types during Planned Metro Disruptions. *J. Transp. Eng. A Syst.* **2024**, *150*, 04024069. [CrossRef]
3. Zhou, T.; Wu, W.; Peng, L.; Zhang, M.; Li, Z.; Xiong, Y.; Bai, Y. Evaluation of Urban Bus Service Reliability on Variable Time Horizons Using a Hybrid Deep Learning Method. *Reliab. Eng. Syst. Saf.* **2022**, *217*, 108090. [CrossRef]
4. Ma, F.; Liu, F.; Yuen, K.F.; Lai, P.; Sun, Q.; Li, X. Cascading Failures and Vulnerability Evolution in Bus–Metro Complex Bilayer Networks under Rainstorm Weather Conditions. *Int. J. Environ. Res. Public Health* **2019**, *16*, 329. [CrossRef]
5. Wu, P.; Xu, L.; Li, J.; Guo, H.; Huang, Z. Recognizing Real-Time Transfer Patterns between Metro and Bus Systems Based on Spatial–Temporal Constraints. *J. Transp. Eng. A Syst.* **2022**, *148*, 04022065. [CrossRef]
6. Naumov, V. Genetic-Based Algorithm of the Public Transport Lines Synchronization in a Transfer Node. *Transp. Res. Procedia* **2020**, *47*, 315–322. [CrossRef]
7. Li, X.; Liao, J.; Wang, T.; Lu, L. Integrated Optimization of Bus Bridging Route Design and Bus Resource Allocation in Response to Metro Service Disruptions. *J. Transp. Eng. A Syst.* **2022**, *148*, 04022050. [CrossRef]

8. Ceder, A.; Golany, B.; Tal, O. Creating Bus Timetables with Maximal Synchronization. *Transp. Res. Part A Policy Pract.* **2001**, *35*, 913–928. [CrossRef]
9. Liu, Z.; Shen, J.; Wang, H. Research on the Generation Model of Regional Bus Timetable Based on Collaborative Departure. *Transp. Syst. Eng. Inf.* **2007**, *7*, 109–113.
10. Chen, X.; Huang, Z.; Kuang, A.; Fan, W. Bus Dispatching Timetable Model with Synergistic Scheduling Based on the Structure of Public Traffic Network. *Syst. Eng.* **2011**, *29*, 108–111.
11. Ibarra-Rojas, O.J.; Rios-Solis, Y.A. Synchronization of Bus Timetabling. *Transp. Res. Part B Methodol.* **2012**, *46*, 599–614. [CrossRef]
12. Ibarra-Rojas, O.J.; López-Irarragorri, F.; Rios-Solis, Y.A. Multiperiod Bus Timetabling. *Transp. Sci.* **2016**, *50*, 805–822. [CrossRef]
13. Pang, S. Research on the Maximum Synchronous Transfer Method of Conventional Bus Connecting to Rail Transit Hubs. Master's Thesis, Southeast University, Nanjing, China, 2021.
14. Bo, H.-J.; Dong, R.-J.; Zhang, M.; Chen, Y.-K. Optimization Method of Bus Time Based on Synchronization Diversity. *J. Traffic Transp. Eng.* **2013**, *13*, 79–85.
15. Nesheli, M.M.; Ceder, A.; Gonzalez, V.A. Real-Time Public-Transport Operational Tactics Using Synchronized Transfers to Eliminate Vehicle Bunching. *IEEE Trans. Intell. Transp. Syst.* **2016**, *17*, 3220–3229. [CrossRef]
16. Sun, T. *Study on Maximum Synchronous Transfer of Metro Considering Transfer Passenger Flow*; Huazhong University of Science and Technology: Wuhan, China, 2016.
17. Hu, B.; Zhao, H.; Sun, X.; Wang, D.; Liu, N. A Model of Synchronous Transfer between Urban Bus Line and Rural Passenger Line. *J. Highw. Transp. Res. Dev.* **2016**, *36*, 144–150.
18. Qi, Y. *Research on Optimization of Regional Bus Synchronous Transfer*; Lanzhou Jiaotong University: Lanzhou, China, 2021.
19. Shi, Y.; Guan, X.; Yan, Z. Evaluation of Urban Rail–Bus Transfer Efficiency Considering Built Environment Characteristics. *J. Railw. Sci. Eng.* **2023**, *20*, 1242–1249.
20. Shen, J.; Zhao, J.; Gao, Y. Interval Prediction of Metro-to-Bus Transfer Passenger Flow Probability Based on Travel Chain Characteristics. *J. Southeast Univ. (Engl. Ed.)* **2022**, *38*, 408–417.
21. Zheng, Y.; Gao, L.; Chen, X. Investigating Influencing Factors on Metro-bus Transfer Demand Incorporating Spatial Heterogeneity Based on Multi-source Data. *J. Transp. Syst. Eng. Inf. Technol.* **2023**, *23*, 128–138. [CrossRef]
22. He, Q.; Feng, Y.; Qian, Y.; Lu, X.; Zeng, J.; Wei, X.; Li, K.; Peng, Y. A Hybrid Improved Atom Search Optimization Algorithm Optimizes BiGRU for Bus Travel Speed Prediction. *Mathematics* **2026**, *14*, 856. [CrossRef]
23. Hu, S.; Ji, M.; Chang, Z.; Wang, H.; Kong, X. An improved particle swarm optimization algorithm based urban rail passenger flow prediction model: A case study in Beijing, China. *Digit. Transp. Saf.* **2025**, *4*, 101–107. [CrossRef]
24. Xing, S.; Guo, J.; Qin, Y.; Jia, L.; Wang, Y.; Jiang, S. Joint Optimization of Passenger Flow Control and Train Skip-Stopping for Overcrowded Metro Lines: A Multi-Agent Reinforcement Learning Approach. *Urban Rail Transit* **2026**, *12*, 38–66. [CrossRef]
25. Jiao, Q.; Yu, Q.; Chen, X.; Cheng, L. Joint Optimization of Metro Travel Reservation and Compartment Capacity Allocation for an Overcrowded Metro Line. *Transp. Lett.* **2025**, *17*, 281–294. [CrossRef]
26. Yin, Y.; Li, D.; Han, Z.; Dong, X.; Liu, H. Maximizing Network Utility While Considering Proportional Fairness for Rail Transit Systems: Jointly Optimizing Passenger Allocation and Vehicle Schedules. *Transp. Res. Part C Emerg. Technol.* **2022**, *143*, 103812. [CrossRef]
27. Cao, Z.; Ceder, A.; Li, D.; Zhang, S. Optimal Synchronization and Coordination of Actual Passenger-Rail Timetables. *J. Intell. Transp. Syst.* **2019**, *23*, 231–249. [CrossRef]
28. Qu, H.; Wang, Z.; Liu, X. Optimizing Integrated All-Stop, Express, and Short-Turn Services on a Metro Line with Capacity Constraint Considering Passenger Spatio-Temporal Path Choice. *Transp. Res. Rec.* **2023**, *2677*, 1525–1541. [CrossRef]
29. Wahaballa, A.M.; Kurauchi, F.; Yamamoto, T.; Schmöcker, J.D. Estimation of platform waiting time distribution considering service reliability based on smart card data and performance reports. *Transp. Res. Rec.* **2017**, *2652*, 30–38. [CrossRef]
30. Xie, X.; Leurent, F. Comparison of passenger walking speed distribution models in mass transit stations. *Transp. Res. Procedia* **2017**, *27*, 696–703. [CrossRef]
31. Mirjalili, S.; Mirjalili, S.M.; Lewis, A. Grey Wolf Optimizer. *Adv. Eng. Softw.* **2014**, *69*, 46–61. [CrossRef]
32. Faris, H.; Aljarah, I.; Al-Betar, M.A.; Mirjalili, S. Grey Wolf Optimizer: A Review of Recent Variants and Applications. *Neural Comput. Appl.* **2017**, *30*, 413–435. [CrossRef]
33. Wang, Z.; Hu, S.; Chen, Z.; Li, X.; Huang, Z.; Pan, H. Coordinated Optimization of Late-Night Metro Timetables with Selective Skip-Stop Strategy: A Hybrid GWO-CNN Approach Balancing OD Accessibility and Maintenance Needs. *Systems* **2026**, *14*, 11. [CrossRef]
34. Mobaraki, M.M.; Roghani Araghi, A.; Noorollahi, Y. Optimization of Urban Metro Scheduling for Reducing Travel Time and Enhancing Transportation System Efficiency. *Urban Dev. Policy Mak.* **2025**, *2*, 17–30. [CrossRef]
35. Cui, Y.; Yu, Q.; Wang, C. Headway Optimisation for Metro Lines Based on Timetable Simulation and Simulated Annealing. *J. Adv. Transp.* **2022**, *2022*, 7035214. [CrossRef]

36. Yu, J.; Xie, Z.; Dong, Z.; Song, H.; Su, J.; Wang, H.; Xiao, J.; Liu, X.; Yang, J. Intelligent Bus Scheduling Control Based on On-Board Bus Controller and Simulated Annealing Genetic Algorithm. *Electronics* **2022**, *11*, 1520. [CrossRef]
37. Kirkpatrick, S.; Gelatt, C.D.; Vecchi, M.P. Optimization by Simulated Annealing. *Science* **1983**, *220*, 671–680. [CrossRef] [PubMed]
38. Wang, Y.; Li, D.; Cao, Z. Integrated timetable synchronization optimization with capacity constraint under time-dependent demand for a rail transit network. *Comput. Ind. Eng.* **2020**, *142*, 106374. [CrossRef]